Preprints (www.preprints.org) | NOT PEER-REVIEWED | Posted: 8 August 2018 doi:10.20944/preprints201808.0152.v1

Article

Thermography Quantification of Human Perfusion Thermal Signature

Abbas K. ALZubaidi [1,*], Ahmed F. Hussein [2], Mena Basil [3], Qais Ahmed Habash [2]

[1] Biomedical Engineering Division, University of Saskatchewan, Saskatchewan, Canada
[2] Biomedical Engineering Departement, AlNahrain Univeristy, Baghdad, Iraq
[3] Al-Israa University College, Baghdad, Iraq
* Correspondence: aba658@mail.usask.ca; Tel.: +1-431-777-9679

Abstract: Blood perfusion quantification is important vital parameters in different diagnostic procedure, using infrared thermography imaging; it is reliable to use this technique as non-contact, non-invasive blood flow measurement method. Therefore, we developed a measurement protocol for blood flow over the arm's anterior surface. By using the superficial brachial and radial veins to be monitored under the impact of cold-excitation of (2 °C to 5 °C), the blood perfusion signal was detected using thermal imager of long-wave infrared spectral range (LWIR, 7μm - 14 μm). The simulation of Penne's bioheat transfer equation was performed to be compared with results obtained from the infrared thermography. Furthermore, the proposed blood flow monitoring using external adjusting of the excitation temperature, by using (cold-compress, or cold air-stream) applied to the region under testing. The signal detected resembles to the hemodynamic pulse of the superficial veins, in the definition of systolic and diastolic phases of the cardiac cycle. Moreover, statistical analysis applied to the BFIRT signals from 24 subjects to estimate the skin's mean temperature after recovery from the thermal excitation.

Keywords: Infrared thermography, blood perfusion signal, thermal excitation, bioheat transfer, Pennes equation, Active thermography imaging

1. Introduction

Every single object emits its thermal radiation energy when the object's temperature above zero-Kelvin (-273.15 °C). Therefore, for the human body, at a temperature of 310 degrees Kelvin, radiation is maximal in the wavelength range of several microns[1,2]. The intensity here is so sufficient, so that standard infrared (IR) imaging technology can be used for detection and identification of various thermal-related phenomena [1,3,4]. Registration of the distribution of human skin temperature, a technique known as thermography, is a well-developed imaging modality in medical practice [5–7]. However, the distribution of skin temperature determined by standard techniques gives only limited information, accordingly, the classical thermography has been useful in the diagnosis of very few diseases, but in contrast, it could detect several physiological phenomena generates heat energy [8].

As general, the localized skin surface cooling can cause blood flow vasoconstriction stimulated by non-adrenergic sympathetic nerves. This localized stressful cooling could be a reliable diagnostic means by infrared thermographers to identify clinically significant alterations in response of skin blood perfusion. Using a cold challenge test, Researchers in [9–11], developed a vasoplasticity test for Raynaud's syndrome based on the temperature gradient in the hand following a cold-water immersion (20 °C for 60 seconds interval). In addition, cold stress testing and IR imaging has also been used to evaluate blood perfusion thermal patterns in patients with carpal tunnel syndrome pre- / post-surgery and sport traumas [12].

Skin blood perfusion and vasodilatation in response to local warming is stimulated by the release of sensory nerve neuropeptides or the non-neural stimulation of the cutaneous arteriole by nitric oxide (NO)

© 2018 by the author(s). Distributed under a Creative Commons CC BY license.

Preprints (www.preprints.org) | NOT PEER-REVIEWED | Posted: 8 August 2018 doi:10.20944/preprints201808.0152.v1

[13,14]. Thermographic imagers have exploited this localized warming response to provide a skin blood perfusion challenge [15,16]. Generally, the use of cold excitation is one of the stable methods for the skin blood perfusion measurement [17–19].

A popular device that belongs to this category is the piezoelectric transducer. It is attached to the finger of a subject and converts local blood pressure variations, associated with cardiac activity, to a electromotive (emv) signal and thermography[20] or even microscopic-like imaging [21]. This is a reliable method, but it is sensitive to motion. The Doppler ultrasound is a more advanced technology that is used to collect blood velocity spectra. Several investigators first strating to recover the full pulse waveform of the carotid and cerebrovascular vessels based on the spectral information of blood velocity [22–24]. Ultrasound imaging measurements still require contact between the probe and subject, in addition to, using of a conductive gel to enhance wave transmission.

Photoplethysmography (PPG) is considered as alternative pulse measurement method that exploits upon the dermal optical properties [25]. For this purpose, near-infrared light is emitted into the skin. More or less light is absorbed, depending on the blood volume in the skin. Consequently, the backscattered light corresponds to the variation of the blood volume associated to the cardiac pulse (see Fig. 1). PPG is used widely to measure the pulse waveform [26], pulse wave reflection [27], cutaneous (dermal) perfusion [28], and capillary micro-circulation [29,30].

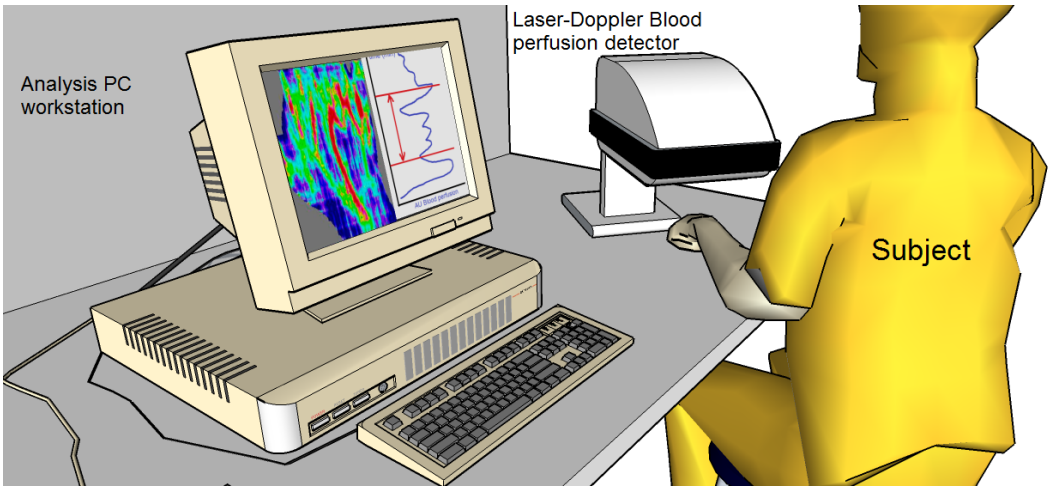

Figure 1. First measurement setup of the Doppler-laser blood perfusion imaging system prototyped by OxyLab® LDF instrumentation (Florida, USA), where the laser irradiation of the field of view and sensing temperature changes of blood flow using Doppler flowmetry unit.

Recently, several researchers have proposed a series of bioheat and statistical models that in combination with customized highly sensitive thermal imaging hardware can measure various physiological variables at several feet away from the subjects. These include contact-free measurements of perfusion [31], vessel blood flow [32], and breathing rate [33]. Since majority of these methods are based on passive imaging are safe and suitable for long observation periods.

2. Methodology and Imaging Setup

Thermography imaging makes use of the infrared (IR) spectral band of the electromagnetic spectrum. Infrared spectrum involves four bands: near infrared (0.75 μm - μm 3), middle infrared (3 μm - 6 μm), far infrared (6 μm -15 μm) and extreme infrared (15-100 μm) which are defined based on ISO-20473 scheme and DIN.5031 part7, 1984-01 (see Fig. 2). The infrared thermal cameras are passive (emits no energy), but merely collects the thermal radiation emitted from the surface of the human body [2,3].

The IR camera used in this paper operates in the long-wave infrared (LWIR) spectral range. The cardiac cycle

Preprints (www.preprints.org) | NOT PEER-REVIEWED | Posted: 8 August 2018 doi:10.20944/preprints201808.0152.v1

is composed of two distinct phases (systolic) and (diastolic). Basically, the setup consisted of a blood pressure measurement (as ground truth) prior to the infrared thermography imaging, additionally, the cold compress applies to the anterior surface of the arm with average excitation temperature reached (5 °C). The average time for cold-stress excitation is about 10 seconds, while this selected time interval to develop moderate skin blood flow response. Basically, the infrared thermal camera (SatIR, G96 High resolution 640x480 thermal detector, Guangzhou, China) with spectral bandwidth of 8 μm - 14 μm over the EM spectrum (see Fig. 2 and Fig. 3). Furthermore, the measurement performed under controlled room temperature. The data analysis and simulation for Bioheat transfer equation was done with MATLAB 2017ő (MathWorks, Natik, MA). Moreover, the statistical analysis for the mean and variance of the BFIRT signals was performed with Statistical toolbox in MATLAB platform

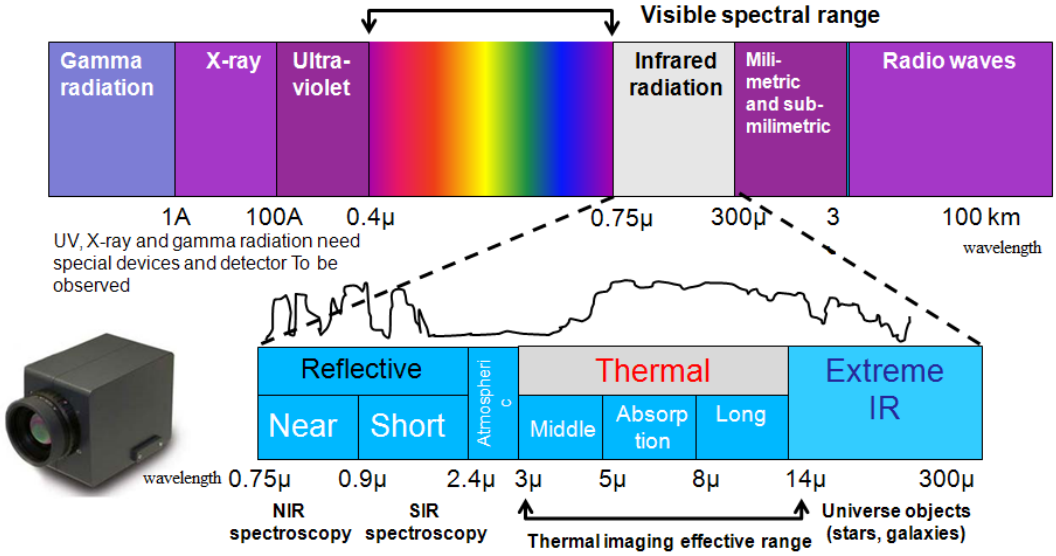

Figure 2. Infrared spectral bandwidths near infrared (NIR), Short-wave infrared (SWIR), Middle wave infrared (MWIR), and Long-wave infrared (LWIR), within the electromagnetic spectrum

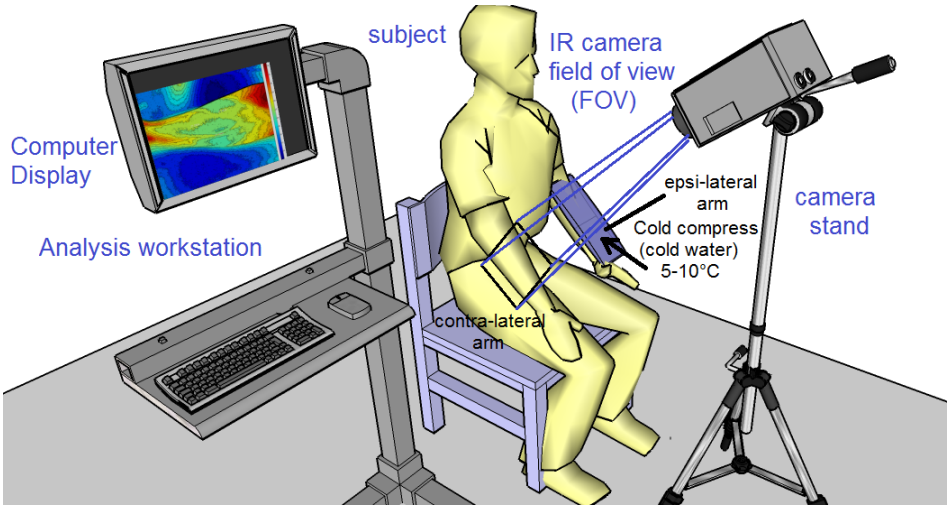

Figure 3. Anatomical view of (a) superficial veins which more apparent with infrared thermography imaging, the most important veins to be visualize is the Basilic vein, (b) the clinical setup for the blood flow measurement with infrared thermography imaging with blood pressure monitoring technique.

Preprints (www.preprints.org) | NOT PEER-REVIEWED | Posted: 8 August 2018 doi:10.20944/preprints201808.0152.v1

3. Physiological parameters

To specify the physiological parameters to be considered in active thermography imaging, we defined the blood flow, perfusion and blood pressure as main hemodynamic index to be monitored in the methodology of this research. Blood flow and pressure set to be measured using gold-standards clinical methods (Doppler ultrasound imaging and Digital blood pressure monitoring device) respectively. These two methods also used as ground truth for the active thermography imaging performed on subject's arm-hand area. It is better to be more specific for the level of measurement with the two methods mentioned previously to get accurate approximation of thermal perfusion signature in the nearby vicinity.

3.1. BFIRT Detection Objective

Blood flow pulsation detection and monitoring are widely used in health care, physical training, sleep-laboratory studies, and psycho-physiological examinations. Various contact measurement methods have been developed to estimate a subject's cardiac pulse. These measurement methods capitalize upon the electro-physiological and mechanical processes associated to the heart activity and blood circulation. The gold standard for pulse measurement is Electrocardiography (ECG) and Oxygen saturation photoplethysmography technique [26,34].

The BFIRT thermal signature origin is based on the sympathetic response to the cold excitation applied to the skin and beneath blood vessel (i.e. superficial veins and arteries) [35,36]. In which different heat transfer mode interaction will be takes place to compensate against the heat loss through forced conduction between the cold media and the blood vessels (see Fig. 4). Hypothesis beyond this research is that, volumetric response of the venous wall to a heat variation causes redistribution of heat along the vein. These heat variations are further passed to the skin surface, where they can be registered by IR-thermal camera [17,37].

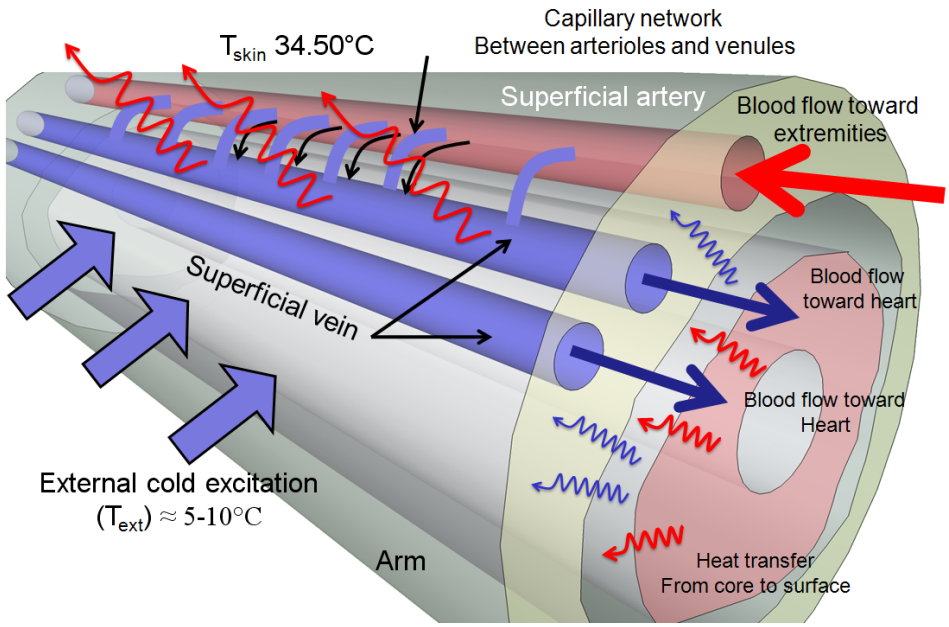

Figure 4. 3D representation of a small tissue volume perfused by a single artery and vein pair. The tissue region is perfused via a capillary network bifurcating from the transverse arterioles, and the blood is drained by the transverse venules.

Unfortunately, this BFIRT signal profile is impractical on raw thermal imagery [38]. Irrelevant heat patterns on the skin destroy or dramatically corrupt thermal patterns produced by venous pulse propagation. In addition, the blood pressure is high in artery than vein and this causing blood and heat flow slower in venous compartment than the arterial one. Given that, there are several factors which affect the BFIRT signal,

Preprints (www.preprints.org) | NOT PEER-REVIEWED | Posted: 8 August 2018 doi:10.20944/preprints201808.0152.v1

such as regional blood flow from the neighboring veins, highly tissue perfusion rate at the onset of thermal excitation[39]. Therefore, selection of the defined vessel profile will minimize the effect of such disturbance.

3.2. Penne's bioheat transfer model

It is known that one of the primary functions of blood flow in a biological system is the ability to heat or cool the tissue, depending on the relative local tissue temperature. The existence of temperature difference between the blood and tissue is considered as firm evidence of its function to remove or release heat [1,40]. Based on this theory, Pennes (1948) proposed his famous heat transfer model [41], which is called Pennes' bioheat equation [15,42]. Pennes suggested that the effect of blood flow in the tissue be modeled as a thermal source and physical sink term added to the conventional heat conduction equation [43]. The Pennes bioheat equation is given by:

$$\rho c \frac{\partial T}{\partial t} = k_t \nabla T_t + q_{blood} + q_m \tag{1}$$

where q_m is the metabolic heat generation in the tissue, and the second term (q_{blood}) on the right side of the equation considers the contribution of blood flow to the local tissue temperature distribution (see Fig. 5). Therefore, the strength of perfusion source term can be derived as follows.

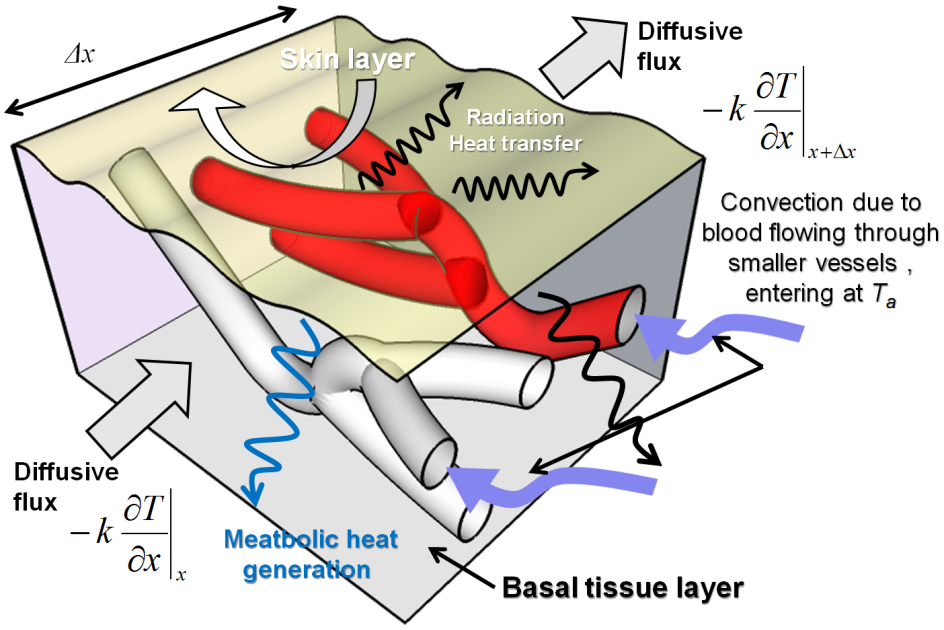

Figure 5. The typical heat transfer in a tissue showing metabolic heat flow generation Q and convective heat transfer due to the passage of blood.

If the assumption that both the artery and vein keep a constant temperature when they pass through this tissue region, the total heat released is equal to the total amount of blood perfusing this tissue volume per second q multiplied by its density ρb, specific heat C_b, and the temperature difference between the artery and vein is given by:

$$q\rho_b c_b (T_a - T_v) = (Q_{in} - Q_{out})\rho_b c_b (T_a - T_v) \tag{2}$$

The volumetric heat generation rate q_{blood} defined as the heat flux rate per unit tissue volume, it is then derived as following:

$$q_{blood} = [(Q_{in} - Q_{out})/V]\rho_b c_b (T_a - T_v) = \omega \rho_b c_b (T_a - T_v) \tag{3}$$

where ω is defined as the amount of blood perfused per unit volume tissue per second. Applying the analogy with gaseous exchange in living tissue, Pennes believed that heat transfer occurred in the capillaries because of their large area for heat exchange [44]. Therefore, the local arterial temperature Ta could be assumed

Preprints (www.preprints.org) | NOT PEER-REVIEWED | Posted: 8 August 2018 doi:10.20944/preprints201808.0152.v1

Table 1. The parameters used in the Penne's bioheat equation simulation.

Constants used in Pennes equation simulation	Numerical value
Tissue Thermal Conductivity, (cal . s^{-1}. cm^{-1}. $°C^{-1}$)	0.0015
Heat Transfer Coefficient (cal . s^{-1} .cm^{-2}. $°C^{-1}$)	0.0002
Arterial Blood Temperature, °C, could be 36.25°C	36.8
Ambient Temperature, (°C)	26.6
Blood Perfusion Rate, min^{-1} (3 mL.100 mL^{-1} .min^{-1})	0 .03
Metabolic Heat Generation, (cal . s^{-1}.cm^{-3})	0.0001
Density of Tissue, assumed same as H_2O, g.cm^{-3}	1
Specific Heat of Tissue, assumed same as H_2O, cal. g^{-1}.$°C^{-1}$	1
Density of Blood, assumed same as H_2O, g. cm^{-3}	1
Specific Heat of Blood, assumed same as H_2O, cal .g^{-1}.$°C^{-1}$	1

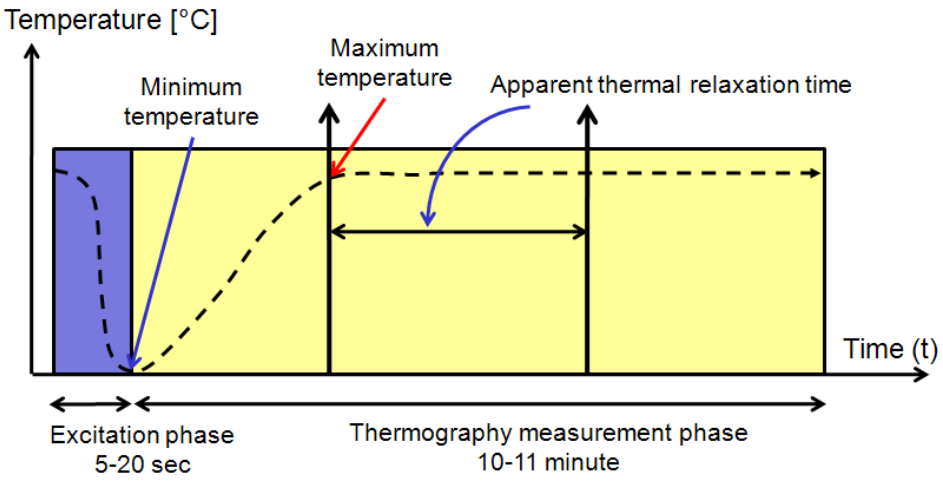

Figure 6. The standardized protocol sequence of the BFIRT signature measurement, used for developing excitation response of thermo-regulatory system

as a constant and equal to the body core temperature T_c [36,45]. As for the local venous blood, it seems reasonable to assume that it equilibrates with the tissue in capillary network and enters the venules at local tissue temperature [30]. The parameters and constants of the Pennes equation used in the simulation as listed in table. 1. Therefore, these simulations paradigms (see Fig. 6) used for comparison between the theoretical response from Pennes equation and the experimental data acquired from the BFIRT signal based on infrared thermography.

As with any cooling procedure, which BFIRT use the conductive based one, commonly proposed mechanisms relate to an increase in circulatory volume and therefore an improved muscle blood flow [2,46]. The resultant peripheral vasoconstriction following changes in skin temperature from cooling and closing of local vasculature promote a larger central circulatory reserve that may be beneficial to reduce cardiac stress due to the increased venous return and stroke volume (SV) [41,47]. While the cardiovascular explanation is certainly plausible of the limited studies that have investigated post-exercise cooling [48], few studies report any differences in heart rates that are not explained by the passive nature of cold water immersion or differences in any cardiovascular measure during ensuing bouts of exercise [39,49].
It is also questionable that the increase in central blood volume resulting from cooling is sufficient to result in changes of hemodynamic function [20,43]. Furthermore, it seems somewhat counter-intuitive that to cool the periphery to increase the central blood volume allows a greater reserve to then re-direct back to the peripheral musculature to aid recovery of an area that is under local vasoconstriction (see Fig. 7). Finally, as

Preprints (www.preprints.org) | NOT PEER-REVIEWED | Posted: 8 August 2018 doi:10.20944/preprints201808.0152.v1

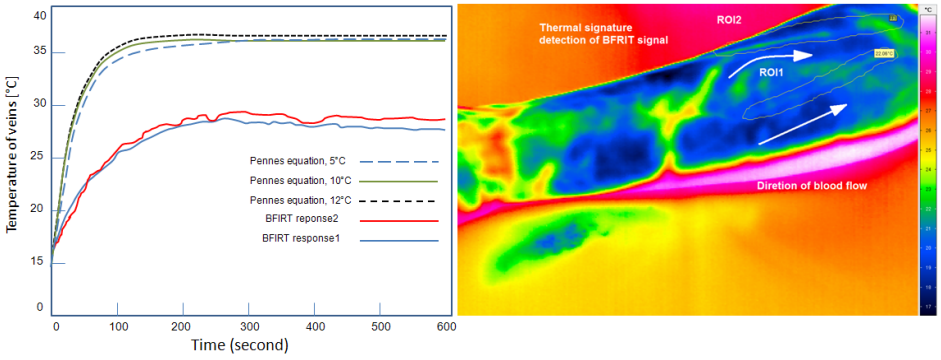

Figure 7. Transient solution of Penne's bioheat heat equation, simulated for constant parameter values in the absence of thermal spatial effects.

previously mentioned tissue oxygenation and blood volumes have been reported to be reduced with cooling in non-exercising single limb models and remain that way for up to 60 min post-cooling phase [40,50].

4. Mathematical formulation of controlled thermal stress of superficial vein

Similar to the work in [12,51] which proposed the natural response model of the fingertips to exposure to a cold environment to identify a diagnostic parameter derived by the physiology of such a response. The thermal recovery following a cold stress is driven by thermal exchange with the environment, transport by the incoming blood flow, conduction from adjacent tissue layers, and metabolic processes [19,32]. The finger temperature is determined by the net balance of the energy input/output [52]. The more significant contributes come from the input power due to blood perfusion and the power lost to the environment:

$$\frac{dQ}{dt} = -\frac{dQ_{env}}{dt} + \frac{dQ_{ctrl}}{dt} \tag{4}$$

In absence of thermoregulatory control, fingers exchange heat only with the environment: in this case, their temperature T_{exp} follows an exponential pattern with time constant τ given by

$$\tau = \frac{\rho.c.V}{h.A} \tag{5}$$

where ρ is the mass density, c the specific heat, V the finger volume, h is the combined heat transfer coefficient between the finger and environment, (A) is the finger's surface area [53]. Generally, a controlled thermal stress applied to the region of interest and the surrounding tissue permits to study and model the response of the region itself [54]. The most important terms involved in the thermal energy balance during recovery are the heat storage in the tissue, heat clearance by blood perfusion and convective heat exchange with the environment, as described by the following equation:

$$\frac{\partial T}{\partial t}\rho \cdot C \cdot V = h \cdot A(T_0 - T) + \rho_{bl} \cdot C_{bl} w_{bl}(t) \cdot (T_{bl} - T) \tag{6}$$

where subscripts (o) and (bl) designate the properties of the environment and blood, respectively, while (ρ) is the density, (c) is the specific heat, (V) is the volume, (T) is the temperature, (t) is the time, (h) is the combined heat transfer coefficient between the skin and environment, (A) is the surface area, and (w) is the blood perfusion rate [8]. The initial condition for Eq. 3 will be as follows: $T=T_i$, for t=0, where T_i is the skin temperature and t = 0 is the time at recovery starting phase [35].
Generally, Eq.6 can be easily integrated under the assumption of constant blood perfusion rate wbl and blood temperature T_{bl}, yielding

$$T(t) = \frac{W.(T_{bl} - T_o)}{W+H} + \left(T_i - T_o - \frac{W.(T_{bl} - T_o)}{W+H}\right).e^{-(W+H).t} + T_o \tag{7}$$

Preprints (www.preprints.org) | NOT PEER-REVIEWED | Posted: 8 August 2018 doi:10.20944/preprints201808.0152.v1

Eq.7, with the assumption of constant blood perfusion, relates the time to reach a pre-set temperature to the local thermal properties and to local blood perfusion. In the meaning, that W and H are the weighting parameters of Eq. 6.

5. Bioheat distribution inside blood vessels

For approximation, the heat transfer inside the blood vessel (i.e. the superficial veins), a detailed analysis of the heat transfer between the blood vessel wall and the mixed mean temperature of the blood (T_b) can be done using standard heat transfer methods as following definition:

$$q'(s) = h\pi d(T_w(s) - T_b) \tag{8}$$

where d is the vessel diameter, $T_w(s)$ is the vessel wall temperature, and the convective heat transfer coefficient h may be found from different investigations [55–57] recommendation that in basis of Nusselt's number (NuN)[58,59] and Graetz number (GN) [49,60,61].

$$Nu_D = \frac{hd}{k_b} = 4 + 0.155\exp(1.56\log_{10} Gz)\,,\; Gz < 10^3 \tag{9}$$

where Gz is the Graetz number defined as follows:

$$G_z = \frac{\rho_b c_b \bar{u} d^2}{k_b L} \tag{10}$$

where L is the vessel length, and ρb cb are the blood density and heat capacity of the blood, respectively. Therefore, the exponential term in this equation can be easily identified in the simulation response as the total heat transfer inside blood vessel (see Fig. 8 and Fig. 9). The Onset of temperature distribution for cold-excitation compensation, and the vasodilatation response of the superficial vein are well differentiated after the first minute of excitation application (see Fig. 8).

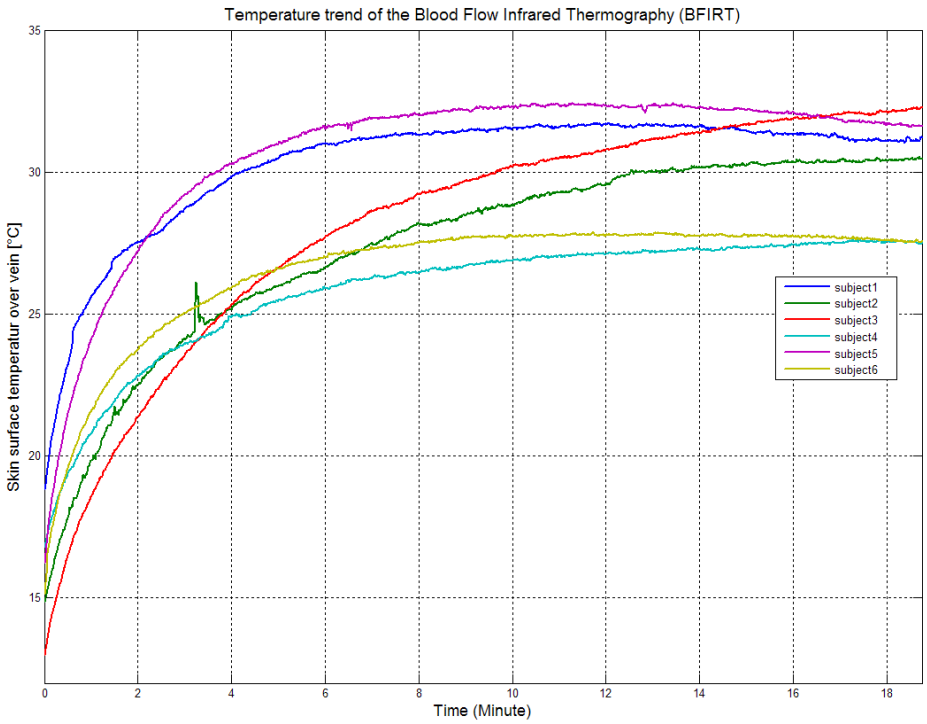

Figure 8. Temperature distribution plot over the specific ROI around the arm superficial veins, the settling time for turning.

Preprints (www.preprints.org) | NOT PEER-REVIEWED | Posted: 8 August 2018 doi:10.20944/preprints201808.0152.v1

This response can be well formulated with moderate thermal excitation (e.g. cold-water or cold-air stream). Fundamentally, the thermal response will vary individually and from vessels to another according to different characteristics of the venous plexus in the forearm (see in Fig. 9). This dissimilarity in the response time and venous thermal signature could be used as differential distinctiveness for human superficial vascular plexus, which may be used as biometric term in the future (see Fig. 9).

Table 2. Comparison of main parameters extracted from the BFIRT measurement

Subj	BP_{mean} ±2 mmHg	T_{skin} ±0.05°C	$T_{ROI-min}$ ±0.05 °C	Stabiliz. time (minute)
1	79	34.23	14.23	10.23
2	75	34.01	13.84	11.06
3	71	35.87	14.29	10.78
4	85	34.37	13.36	11.33
5	64	34.05	13.73	11.28
6	64	34.73	14.29	12.69
7	77	34.80	14.02	10.15
8	84	34.23	14.11	10.23
9	85	33.17	13.82	11.45

Similarly, the possible future application of superficial vein thermal response (SVTR) detection is developing superficial veins navigation with other imaging modalities (SO_2) perfusion imaging application. As well as, applying this method for other physiological and clinical test (e.g. contra lateral old stress for pharmaceutical evaluation), and prediction of pain onset with aid of infrared thermography imaging. Moreover, the use of cold stress in breast cancer detection as in mammothermography imaging, to initiate neurological reflex.

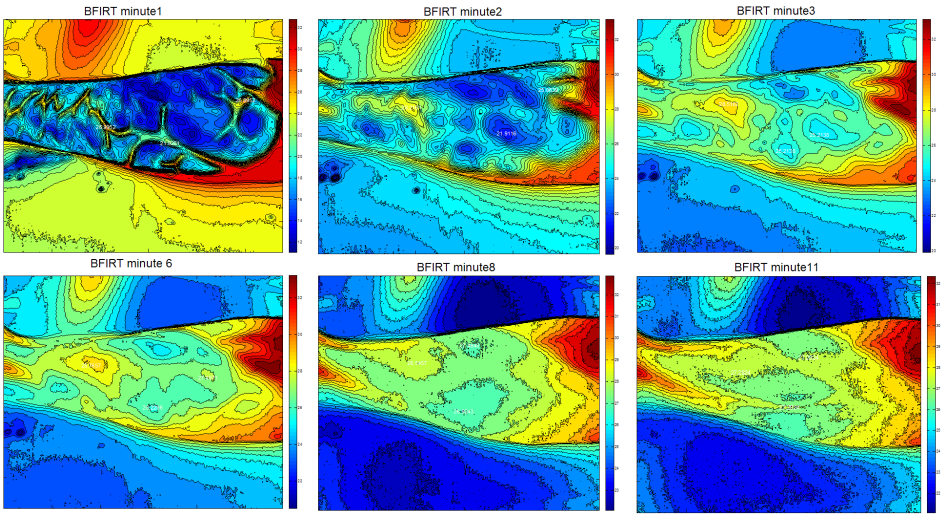

Figure 9. Contouring plot of the infrared thermography images of the BFIRT protocol applied for subject in 11 minute interval, showing the variation of temperature mapping during the initial phase of cold-excitation and following thermal relaxation time.

Preprints (www.preprints.org) | NOT PEER-REVIEWED | Posted: 8 August 2018 doi:10.20944/preprints201808.0152.v1

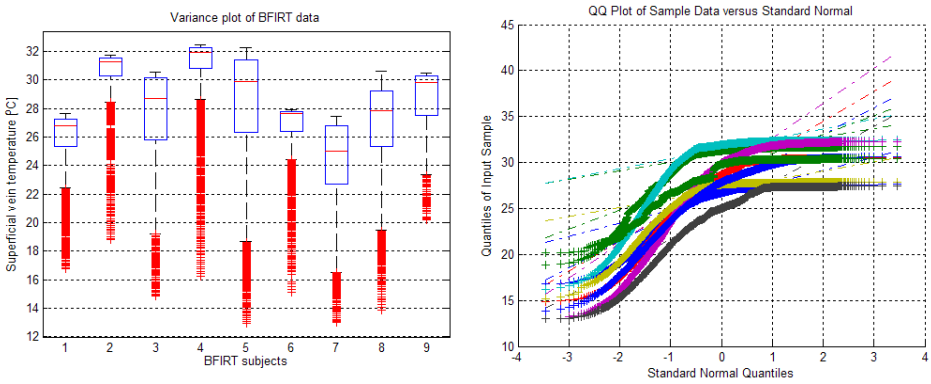

Figure 10. Box plot of the BFIRT data for 9 subjects (a), showing the variation of mean temperature for superficial veins, (b) the QQ-plot (BFIRT input sample vs. standard normal) of the BFIRT data

6. Ultrasonography and Doppler finding

Principally, we use GE vivid 7 Ultrasound scanner with doppler module (@ 3.5 MHz - 4 MHz) to acquire successive Doppler sonography of the cubital region (fossa) and anterior surface of the forearm to see the changes in blood flow prior to the cold-stress measurement and after application of this stress for each individual participated in the study. Figure below illustrates the samples of echo-sonography of the cubital fossa region and forearm. The doppler-sonography imaging proves no alteration on the blood flow patterns despite the cold stress and thermal signature variation of the forearm, which indicates the irrelevance between superficial perfusion and deep vascular blood flow at this level of measurement. Therefore, as conclusion for blood perfusion signal acquired from skin, it is convenient to use this physiological-thermal signature as biometric indicator in several application.

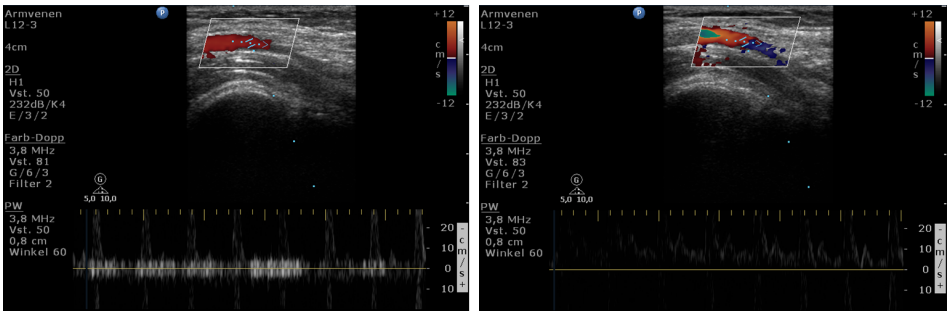

Figure 11. Box plot of the BFIRT data for 9 subjects (a), showing the variation of the mean temperature of superficial veins, (b) the QQ-plot (BFIRT input sample vs. standard normal) of the BFIRT data

7. Discussion and Conclusion

Most notable among the garnered results is the consistency of the general trend of responses between subjects; each subject had almost the same trend in reaction to the excitation, making the response predictable. The response itself leans heavily toward first order dynamics, suggesting a quick rise followed by a slowing and stabilization in all subjects, as expected. This lends further credence to the possibility of a modified Pennes' equation accurately depicting the results. The presence of skin, arteries, and other surrounding tissue also reveals itself it the dissimilarities from the Pennes' solution; any data collected is tempered due to the measurement being made through multiple layers of tissue, as well as the presence of other heating and cooling elements around the vein. The evidence of persistent rise time and overshoot across veins from one subject, however, especially across multiple trials, reveals that the physiological reaction is consistent across the body.

Given that, the consistency of physiological responses, it may also be possible to predict complications before they arise through constant monitoring of the human subject or in infant inside NICU wards for future

Preprints (www.preprints.org) | NOT PEER-REVIEWED | Posted: 8 August 2018 doi:10.20944/preprints201808.0152.v1

application. Furthermore, the presence of overshoot in all patients suggests that it is a common reaction; given this, it may also be possible to treat preemptively by anticipating the maximum and final temperatures of the human given a rate of increase in the temperature over a specified time (see Fig. 10).

Primarily, more trials should be performed to verify the outcomes of blood perfusion signature as a standard biometric measure and to solidify ground for reliable analytical extrapolations. Furthermore, the most lacking aspect currently present is the absence of enough data beyond the ten minutes interval; since all subjects barely reached normal skin temperature shortly after this interval and may be there are also instantaneous vascular changes not detected with the thermal camera. Additionally, the full length of the trials must be extended to get an accurate signal for more pattern classification and learning as well by using AI and ML computation platforms.

Some of future steps to be taken for optimizing this method of thermal perfusion signature such as, (1) Reconstruction of spatio-temporal filter for the blood perfusion signature signal that can reliably to create a smoother BFIRT signal, removing noise from surrounding tissue and hair, to allow for more precise calculations and better predictability of the model; (2) Extended data evaluation will greatly aid in the construction of the filter. (3) Implementation of this method under good medical ethical aspects, to be perform on preterm infants, because applying such cold excitation to critically infant, will cause a considerable thermal shock and may lead to clinical consequences. Although, the authors noticed in some of experiment were the nurse's hand interact with baby have more than 10 °C gradient between the nurse's and baby's skin. Moreover, a proper and moderate cold excitation with medical ethic approval should be prepared to conduct such infrared thermography on neonates for detection any vascular anomalies in neonate's at early stage.

Author Contributions: "Conceptualization, A.A. and A.H.; wrote the whole paper including Methodology, Software, Validation, Q.H., and A.A.; Formal Analysis, M.B.; Investigation, M.B.; Resources, Q.H.; Data Curation, Q.H.; Writing—Original Draft Preparation, A.A.; Writing—Review & Editing, A.H.; Visualization, M.B.; Supervision, Q.A.; Project Administration, M.B.; Funding Acquisition, A.H.".

Funding: This research received no external funding.

Conflicts of Interest: The authors declare no conflict of interest.

References

1. Clark, R.P. Human Skin Temperature and Its Relevance in Physiology and Clinical Assessment. *Recent Advances in Medical Thermology* **1984**. doi:10.1007/978-1-4684-7697-2_2.
2. Diakides, N.; Bronzino, J. Medical Infrared Imaging, 2007. doi:10.1201/9781420008340.
3. Caniou, J. Infrared detection. *Passive Infrared Detection* **1999**. doi:10.1007/978-1-4757-6140-5_1.
4. Holst, G.C. *Common sense approach to thermal imaging*; SPIE: Bellingham, 2000. Literaturangaben.
5. Vardasca, R.; Simoes, R. Current Issues in Medical Thermography. *Topics in Medical Image Processing and Computational Vision* **2013**. doi:10.1007/978-94-007-0726-9_12.
6. Abbas, A.K.; Leonhardt, S. Intelligent neonatal monitoring based on a virtual thermal sensor. *BMC Medical Imaging* **2014**, *14*, 1. doi:10.1186/1471-2342-14-9.
7. Knobel, R.B.; Guenther, B.D.; Rice, H.E. Thermoregulation and thermography in neonatal physiology and disease. *Biological research for nursing* **2011**, *13*, 274–282.
8. Kyle, D.; Allen, J.; Overbeck, K.; Stansby, G. Exploratory Thermal Imaging Assessments of the Feet in Patients with Lower Limb Peripheral Arterial Disease. In *Application of Infrared to Biomedical Sciences*; Springer, 2017. doi:10.1007/978-981-10-3147-2_14.
9. Leeuwen, G.M.J.V.; Kotte, A.N.T.J.; Bree, J.D.; der Koijk, J.F.V.; Crezee, J.; Lagendijk, J.J.W. Accuracy of geometrical modelling of heat transfer from tissue to blood vessels **1997**. *42*, 1451–1460. doi:10.1088/0031-9155/42/7/017.
10. SINGH, S.; REPAKA, R. Numerical investigation of convective cooling in minimizing skin burns during radiofrequency ablation of breast tumor. *Sādhanā* **2018**, *43*, 1. doi:10.1007/s12046-018-0872-4.
11. Piérard, G.E.; Hermanns-Lê, T.; Piérard-Franchimont, C. Skin Tensile Strength in Scleroderma. In *Agache's Measuring the Skin*; Springer, 2017. doi:10.1007/978-3-319-32383-1_133.

Preprints (www.preprints.org) | NOT PEER-REVIEWED | Posted: 8 August 2018 doi:10.20944/preprints201808.0152.v1

12. Gil-Calvo, M.; Jimenez-Perez, I.; Pérez-Soriano, P.; Priego Quesada, J.I. Foot Temperature Assessment. In *Application of Infrared Thermography in Sports Science*; Springer, 2017. doi:10.1007/978-3-319-47410-6_10.
13. Soerensen, D.D.; Pedersen, L.J. Infrared skin temperature measurements for monitoring health in pigs: a review. *Acta Veterinaria Scandinavica* **2015**, *57*, 1. doi:10.1186/s13028-015-0094-2.
14. Ong, V.H.; Denton, C.P. Secondary Raynaud's Phenomenon. *Raynaud's Phenomenon* **2015**. doi:10.1007/978-1-4939-1526-2_8.
15. Lahiri, B.B.; Bagavathiappan, S.; Raj, B.; Philip, J. Infrared Thermography for Detection of Diabetic Neuropathy and Vascular Disorder. In *Application of Infrared to Biomedical Sciences*; Springer, 2017. doi:10.1007/978-981-10-3147-2_13.
16. Vollmer, M.; Möllmann, K.P. Infrared Thermal Imaging, 2017. doi:10.1002/9783527693306.
17. Ring, F.J. Skin Thermal Imaging. *Measuring the Skin* **2016**. doi:10.1007/978-3-319-26594-0_73-1.
18. Deng, Z.S.; Liu, J. Effects of Large Blood Vessels on Temperature Distributions During Simulated Cryosurgery, 2004. doi:10.1115/imece2004-61103.
19. Herrick, A.L.; Wigley, F.M.; Matucci-Cerinic, M. Raynaud's Phenomenon, Digital Ulcers and Nailfold Capillaroscopy. In *Scleroderma*; Springer, 2017. doi:10.1007/978-3-319-31407-5_20.
20. Alpar, O.; Krejcar, O. Detection of Raynaud's Phenomenon by Thermographic Testing for Finger Thermoregulation. *Intelligent Information and Database Systems* **2017**. doi:10.1007/978-3-319-54430-4_46.
21. Humbert, P.; Sainthillier, J.M.; Mac-Mary, S.; Lihoreau, T.; Fanian, F.; Jeudy, A.; Li, L. Skin Capillaroscopy. *Agache's Measuring the Skin* **2016**. doi:10.1007/978-3-319-26594-0_60-1.
22. Antonutto, G.; Girardis, M.; Tuniz, D.; Prampero, P.E. Noninvasive assessment of cardiac output from arterial pressure profiles during exercise. *European Journal of Applied Physiology and Occupational Physiology* **1995**, *72*, 18. doi:10.1007/BF00964109.
23. Böhringer, H.J.; Lankenau, E.; Stellmacher, F.; Reusche, E.; Hüttmann, G.; Giese, A. Imaging of human brain tumor tissue by near-infrared laser coherence tomography. *Acta Neurochirurgica* **2009**, *151*, 507. doi:10.1007/s00701-009-0248-y.
24. Cholewka, A.; Kajewska, J.; Marek, K.; Sieroń-Stołtny, K.; Stanek, A. How to use thermal imaging in venous insufficiency? *Journal of Thermal Analysis and Calorimetry* **2017**, *130*, 1317. doi:10.1007/s10973-017-6141-7.
25. Tamura, T.; Maeda, Y. Photoplethysmogram. In *Seamless Healthcare Monitoring*; Springer, 2018. doi:10.1007/978-3-319-69362-0_6.
26. Gao, L.; ElwellElwell, C.E.; Kohl-Bareis, M.; Gramer, M.; Cooper, C.E.; Leung, T.S.; Tachtsidis, I. Effects of Assuming Constant Optical Scattering on Haemoglobin Concentration Measurements Using NIRS during a Valsalva Manoeuvre. *Oxygen Transport to Tissue XXXII* **2011**. doi:10.1007/978-1-4419-7756-4_3.
27. Nakamura, H. Development of noninvasive measurement of peripheral circulation and its medical application. *Environmental Health and Preventive Medicine* **1997**, *2*, 1. doi:10.1007/BF02931222.
28. Sancibrian, R.; Gutierrez-Diez, M.C.; Redondo-Figuero, C.; Sarabia, E.G.; Benito-Gonzalez, M.A.; Manuel-Palazuelos, J.C. Thermal Imaging-Based Muscular Activity in the Biomechanical Study of Surgeons. *Bioinformatics and Biomedical Engineering* **2016**. doi:10.1007/978-3-319-31744-1_15.
29. Hinze, A.M.; Wigley, F.M. Pharmacotherapy Options in the Management of Raynaud's Phenomenon. *Current Treatment Options in Rheumatology* **2018**, p. 1. doi:10.1007/s40674-018-0102-6.
30. Orbegozo, D.; Mongkolpun, W.; Stringari, G.; Markou, N.; Creteur, J.; Vincent, J.L.; De Backer, D. Skin microcirculatory reactivity assessed using a thermal challenge is decreased in patients with circulatory shock and associated with outcome. *Annals of Intensive Care* **2018**, *8*, 1. doi:10.1186/s13613-018-0393-7.
31. Umapathy, S.; Vasu, S.; Gupta, N. Computer Aided Diagnosis Based Hand Thermal Image Analysis: A Potential Tool for the Evaluation of Rheumatoid Arthritis. *Journal of Medical and Biological Engineering* **2018**, *38*, 666. doi:10.1007/s40846-017-0338-x.
32. Ismail, E.; Merla, A. Modeling Thermal Infrared Imaging Data for Differential Diagnosis. In *Application of Infrared to Biomedical Sciences*; Springer, 2017. doi:10.1007/978-981-10-3147-2_27.
33. Abbas, A.K.; Heimann, K.; Jergus, K.; Orlikowsky, T.; Leonhardt, S. Neonatal non-contact respiratory monitoring based on real-time infrared thermography. *BioMedical Engineering OnLine* **2011**, *10*, 1. doi:10.1186/1475-925X-10-93.
34. Benaron, D.A.; Stevenson, D.K. Resolution of Near Infrared Time-of-Flight Brain Oxygenation Imaging. In *Oxygen Transport to Tissue XV*; Springer, 1994. doi:10.1007/978-1-4615-2468-7_81.

Preprints (www.preprints.org) | NOT PEER-REVIEWED | Posted: 8 August 2018 doi:10.20944/preprints201808.0152.v1

35. Grassl, E.D.; Barocas, V.H.; Bischof, J.C. Effects of Freezing on the Mechanical Properties of Blood Vessels, 2004. doi:10.1115/imece2004-60244.
36. Fasano, A.; Sequeira, A. Blood and Heat Transfer. In *Hemomath*; Springer, 2017. doi:10.1007/978-3-319-60513-5_6.
37. Abbas, A.K.; Heimann, K.; Blazek, V.; Orlikowsky, T.; Leonhardt, S. Neonatal infrared thermography imaging: Analysis of heat flux during different clinical scenarios **2012**. *55*, 538–548. doi:10.1016/j.infrared.2012.07.001.
38. Castro-Ospina, A.E.; Correa-Mira, A.M.; Herrera-Granda, I.D.; Peluffo-Ordóñez, D.H.; Fandiño-Toro, H.A. Fingertips Segmentation of Thermal Images and Its Potential Use in Hand Thermoregulation Analysis. *Hybrid Artificial Intelligent Systems* **2018**. doi:10.1007/978-3-319-92639-1_38.
39. García, A.; Camargo, C.; Olguín, J.; Barreras, J.A.L. Analysis of Risk for Repetitive Work Using Thermography Sensory. In *Advances in Human Factors and Ergonomics in Healthcare and Medical Devices*; Springer, 2018. doi:10.1007/978-3-319-60483-1_24.
40. Chato, J.C. Heat Transfer to Blood Vessels **1980**. *102*, 110. doi:10.1115/1.3138205.
41. Bourantas, G.C.; Joldes, G.R.; Wittek, A.; Miller, K. A Flux-Conservative Finite Difference Scheme for the Numerical Solution of the Nonlinear Bioheat Equation. In *Computational Biomechanics for Medicine*; Springer, 2019. doi:10.1007/978-3-319-75589-2_7.
42. Zhang, Y.; Xie, H.W. The Convective Heat Transfer in Furcated Blood Vessels. *475-476*, 1599–1602. doi:10.4028/www.scientific.net/amm.475-476.1599.
43. Davey, M.; Eglin, C.; House, J.; Tipton, M. The contribution of blood flow to the skin temperature responses during a cold sensitivity test. *European Journal of Applied Physiology* **2013**, *113*, 2411. doi:10.1007/s00421-013-2678-8.
44. Lillicrap, T.; Tahtalı, M.; Neely, A.; Wang, X.; Bivard, A.; Lueck, C. A model based on the Pennes bioheat transfer equation is valid in normal brain tissue but not brain tissue suffering focal ischaemia. *Australasian Physical & Engineering Sciences in Medicine* **2017**, *40*, 841. doi:10.1007/s13246-017-0595-6.
45. Shrivastava, D. Thermal Effects of Blood Vessels. doi:10.1002/9781119127420.ch3.
46. Gold, J.E.; Cherniack, M.; Hanlon, A.; Dennerlein, J.T.; Dropkin, J. Skin temperature in the dorsal hand of office workers and severity of upper extremity musculoskeletal disorders. *International Archives of Occupational and Environmental Health* **2009**, *82*, 1281. doi:10.1007/s00420-009-0450-5.
47. Caballero, A.D.; Laín, S. A Review on Computational Fluid Dynamics Modelling in Human Thoracic Aorta. *Cardiovascular Engineering and Technology* **2013**, *4*, 103. doi:10.1007/s13239-013-0146-6.
48. Thiriet, M.; Delfour, M.; Garon, A. Vascular Stenosis: An Introduction. *PanVascular Medicine* **2015**. doi:10.1007/978-3-642-37078-6_32.
49. Eglin, C.M.; Golden, F.S.; Tipton, M.J. Cold sensitivity test for individuals with non-freezing cold injury: the effect of prior exercise. *Extreme Physiology & Medicine* **2013**, *2*, 1. doi:10.1186/2046-7648-2-16.
50. Amri, A.; Wilkinson, A.J.; Pulko, S.H. Potentialities of Dynamic Breast Thermography. In *Application of Infrared to Biomedical Sciences*; Springer, 2017. doi:10.1007/978-981-10-3147-2_7.
51. Merla, A.; Mattei, P.A.; Donato, L.; Romani, G.L. Thermal Imaging of Cutaneous Temperature Modifications in Runners During Graded Exercise. *Annals of Biomedical Engineering* **2010**, *38*, 158. doi:10.1007/s10439-009-9809-8.
52. Zhmakin, A.I. Heat Transfer In Vivo: Phenomena and Models. In *Handbook of Thermal Science and Engineering*; Springer, 2018. doi:10.1007/978-3-319-26695-4_70.
53. Urakov, A.L.; Kasatkin, A.A.; Urakova, N.A. Change in Local Temperature of Venous Blood and Venous Vessel Walls as a Basis for Imaging Superficial Veins During Infrared Phlebography Using Temperature-Induced Tissue Contrasting. In *Application of Infrared to Biomedical Sciences*; Springer, 2017. doi:10.1007/978-981-10-3147-2_24.
54. Groeneweg, G.; Huygen, F.J.; Niehof, S.P.; Wesseldijk, F.; Bussmann, J.B.; Schasfoort, F.C.; Stronks, D.L.; Zijlstra, F.J. Effect of tadalafil on blood flow, pain, and function in chronic cold Complex Regional Pain Syndrome: a randomized controlled trial. *BMC Musculoskeletal Disorders* **2008**, *9*, 1. doi:10.1186/1471-2474-9-143.
55. Shrivastava, D.; McKay, B.; Roemer, R.B. An Analytical Study of Heat Transfer in Finite Tissue With Two Blood Vessels and Uniform Dirichlet Boundary Conditions **2005**. *127*, 179. doi:10.1115/1.1842788.
56. Xu, P.; Liu, X.; Zhang, H.; Ghista, D.; Zhang, D.; Shi, C.; Huang, W. Assessment of boundary conditions for CFD simulation in human carotid artery. *Biomechanics and Modeling in Mechanobiology* **2018**, p. 1. doi:10.1007/s10237-018-1045-4.
57. Arzani, A.; Dyverfeldt, P.; Ebbers, T.; Shadden, S.C. In Vivo Validation of Numerical Prediction for Turbulence Intensity in an Aortic Coarctation. *Annals of Biomedical Engineering* **2012**, *40*, 860. doi:10.1007/s10439-011-0447-6.
58. Alpar, O.; Krejcar, O. Detection of Irregular Thermoregulation in Hand Thermography by Fuzzy C-Means. *Bioinformatics and Biomedical Engineering* **2018**. doi:10.1007/978-3-319-78759-6_24.

Preprints (www.preprints.org) | NOT PEER-REVIEWED | Posted: 8 August 2018 doi:10.20944/preprints201808.0152.v1

59. Amri, A.; Wilkinson, A.J.; Pulko, S.H. Potentialities of Dynamic Breast Thermography. In *Application of Infrared to Biomedical Sciences*; Springer, 2017. doi:10.1007/978-981-10-3147-2_7.
60. Chen, C. Development of a Heat Transfer Model for Plant Tissue Culture Vessels **2003**. *85*, 67–77. doi:10.1016/s1537-5110(02)00289-1.
61. Deng, Z.S.; Liu, J. Numerical Study of the Effects of Large Blood Vessels on Three-Dimensional Tissue Temperature Profiles During Cryosurgery **2006**. *49*, 47–67. doi:10.1080/10407780500301770.